12th International Conference on Fracture Mechanics of Concrete and Concrete Structures
FraMCoS-12
B.L.A. Pichler, Ch. Hellmich, P. Preinstorfer (Eds)

https://doi.org/10.21012/FC12.1280
TT-F:1

EVALUATION OF COLUMN-BEAM JOINTS AND OPTIMIZATION OF REINFORCING BARS OF RC VIADUCTS BY FEM

KEN WATANABE*, RYO SUZUKI* AND YUKI NAKATA*

* The Railway Technical Research Institute, Structures Technology Division
2-8-38 Hikari-cho, Kokubunji-shi, Tokyo Japan
e-mail: watanabe.ken.08@rtri.or.jp, www.rtri.or.jp/eng/

Key words: Beam-column Joints, Normalized Cumulative Strain Energy, Structural Details

Abstract: In this study, FEM were performed on L-shaped and T-shaped beam-column joints in order to establish a verification method for joints by the finite element analysis (FEM), and an applicability of the damage indices (the second invariant of deviation, and the strain and normalized cumulative strain energy), which have been shown to be applicable to RC beams, columns, slab members, etc., to the joint was investigated. It was confirmed that damage at corner angles was determined earlier than in other cases. The FEM indicated that the damage indices can be used to evaluate the damage to the joints because the cracking and compression damage of concrete can be generally expressed by dividing the joint into sections.

1 INTRODUCTION

The verification of beam-column joints (hereinafter referred to as the joint) of railway viaducts is omitted by complying with the structural specifications for rebars and haunches according to the design standard. If the joint was designed by just follows the structural detail, it lead to the labour saving in the verification, however, it is difficult to deal with the new materials or method because the rage for the application of the detail was small. If the performance: e.g. the cracking load and the load-bearing capacity, were evaluated, the reasonable size and shape of cross-sections and rebars arrangement for the joint will be obtained. The verification method for the joint that is able to select these advantages. To solve the problem related to the design method of RC structures, the verification by the non-linear finite element analysis (FEM) was standardized in the JSCE specifications [1] [2] with the material damage indices for concrete, such as the second invariant of deviatoric strain and the normalized cumulative strain energy. The applicability of the material damage indices has been verified for RC beams, columns, and slabs.

The objective of this study is to develop the verification method for the joint by FEM. The applicability of the damage index and the limit values. To investigate the phenomena that bending bars and hooks affecting the load-bearing capacity of the joint, the authors modelled rebars in the joint by using the discrete bar. The model was verified by comparing with the result of loading tests, such as cracking load and load-displacement relationships, of L-shaped and T-shaped specimens cast as the joints of RC rigid-frame viaducts. [3] Finally, the applicability of damage indices of models using discrete rebars including the case of compressive damage at the inner radius of bending of the joints was examined.

2 DAMAGE INDEX

Saito et al. [2] have proposed the damage index of concrete and rebars based on stress and strain. The damage index has been defined as

the deviatoric strain second invariant $\sqrt{J_2'}$ for tensile damage, and the normalized cumulative strain energy W_n for compressive damage, and stated in the JSCE specifications [1]. These were defined as in Eqs. (1) and (2).

$$\sqrt{J_2'} = \frac{1}{2} e_{ij} e_{ij} \tag{1}$$

$$W_n = \frac{1}{f} \int \sigma_{ij}^c d\varepsilon_{ij} \tag{2}$$

where, e_{ij}: deviatoric strain tensor ($= \varepsilon_{ij} - \varepsilon_{ij}\delta_{ij}/\delta_{ll}$), ε_{ij} : total strain tensor, δ_{ij} : Kronecker's delta, σ_{ij}^c: stress tensor of concrete, $d\varepsilon_{ij}$: strain increment tensor, f: normalization parameter. The value of f is generally the compressive strength of the concrete.

Each damage index was weighted and averaged to reduce the dependency of the element size on the damage index. Here, the averaged damage index $\overline{D}$ was calculated by taking a weighted average of the indices at the Gaussian points contained in a sphere whose radius was the averaging length L centered at each Gaussian point and weighted by distance as in Eq. (3).

$$\overline{D} = \frac{\int_A D \cdot w(x) dA}{\int_A w(x) dA} \tag{3}$$

where, D is the local damage index, and x is the distance from the Gaussian point of interest. Also, $w(x)$ is the weight at distance x, defined as in Eq.(4).

$$w(x) = \begin{cases} 1 - x/L & x \le L \\ 0 & x > L \end{cases} \tag{4}$$

It has been verified that this averaged damage index was evaluated with $\overline{\sqrt{J_2'}}$ =1000 μ, $\overline{W_n}$=1500 μ as limit values when averaged over an averaging length L=150 mm. [1] Henceforth, the averaged damage index is referred to as the damage index in this paper.

3 OVERVIEWS OF ANALYSIS

3.1 Analysis Model

A three-dimensional FEM was performed using the general-purpose FEM code DIANA ver. 10.5. The experimental specimen: L-shaped and T-shaped joints [3][4], where the joint used in a typical railway viaduct was reduced its scale to about 50% was discretized as shown in Figure 1. The concrete was discretized by solid elements. An element size was 31.25 mm. The rebar was the embedded-rebar element considering only stiffness in axial direction, and the bent part of the axial rebar in the L-shaped joint was discretized by about 10-mm to reproduce the curve of the bent anchorage part. In order to reproduce the pin-support used in the experiment, the solid element at the center of rotation of the pin-support and the support of the horizontal and vertical members were connected with rigid beam elements.

The constitutive model of concrete was Parabolic model for the compressive side and Hordijk model for the tensile side. The softening curve of both models were calculated based on the fracture energy by Eqs. (5) and (6) as:

$$G_F = 10(d_{max})^{1/3} \cdot f_c'^{1/3} \tag{5}$$

$$G_{fc} = 8.8\sqrt{f_c'} \tag{6}$$

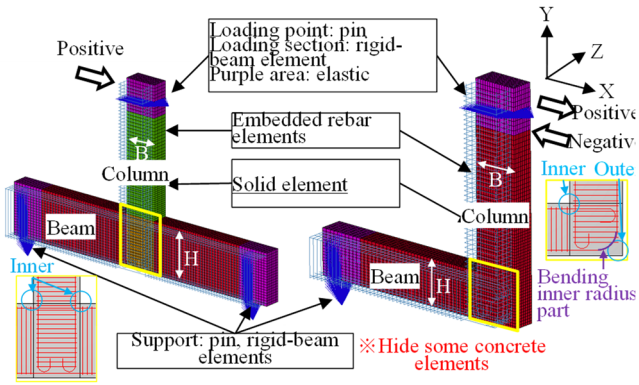

Figure 1 Analysis model.

Table 1 Analysis cases.

Case	Shape	*H*/*B*	Bending inner radius
L-1.0-P3	L	1.0	3ϕ
L-1.0-P10			10ϕ
L-1.6-P3		1.6	3ϕ
L-1.6-P10			10ϕ
T-1.0	T	1.0	
T-1.6		1.6	

* ϕ: diameter of axial rebars, *H*: height of beam (=500mm at *H*/*B*=1.0, =800mm at *H*/*B*=1.6), *B*: height of column (=500mm).

where, G_F : the tensile fracture energy of concrete, d_{max} : the maximum size of coarse aggregate (mm), f'_{ck} : the compressive strength of concrete (N/mm^2), G_{fc} : the compressive fracture energy. The compressive strength: 27 N/mm^2, the tensile strength: 2.6 N/mm^2, and the modulus of elasticity of concrete: 25.9 kN/mm^2 were set in this study.

The axial rebar was set as a linear to avoid flexural yielding in the columns and beams and to evaluate the load-bearing capacity of the joint. The modulus of elasticity was 200 kN/mm^2. The cracks were expressed as the fixed cracks model, and Al-mahaidi model, in which the shear force decreases with the crack width, was applied for shear force transfer at the cracked surface. The bond stress between the rebar and concrete was reduced to 40% of the bond stress proposed by Shima et al. with reference to previous studies. [4][5] The loading method for the L-shape case was monotonic loading in the positive (open) or negative (closed) direction. While the T-shape case was symmetrical, so only one-way loading in the positive direction was used.

3.2 Analysis Case

Table 1 lists the analysis cases. The analysis was performed on L-shaped and T-shaped cases. The cross-sectional height of columns was B=500 mm, and the cross-sectional height of beams were H=500 mm (H/B=1.0) or H=800 mm (H/B=1.6). The length from the support and loading point to the base of the joint, L=1800 mm. The inner radius of bending of the outer axial rebar along the corner of the L-shaped joint was 3 or 10 times of the rebar radius ϕ. The other axial bars were assumed to be semi-circular hooks. The ratio of the rebar p_w in the columns, beams, and joints was all set to 0.57%.

4 LOAD-BEARING MECHANISM OF THE JOINT

To discuss the mechanisms, the strain or stress distribution diagram at the center section of the joint in the Z-direction was investigated in the following section.

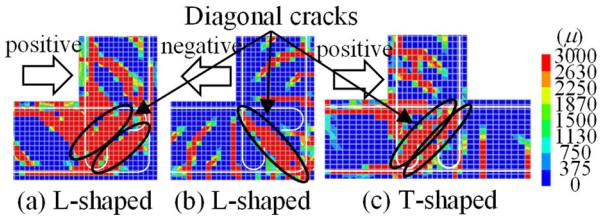

Figure 2 Max. principal strain. (L-1.0-P3, T-1.0)

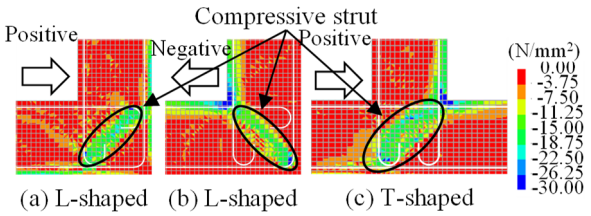

Figure 3 Min. principal stress.

4.1 L-shape case with positive loading

Figure 2(a) shows the maximum principal strain distribution at the maximum positive load. After the observation of flexural cracks in the columns and beams, diagonal cracks were confirmed connecting the compressive fibers of columns and beams. Figure 3(a) shows the minimum principal stress distribution at the maximum positive load. The compression strut occurred along the diagonal cracks and damages the outer base of the columns and beams. Both trends were similar for the case with the inner radius in bending 10ϕ and H/B=1.6.

4.2 L-shape case with negative loading

Figure 2(b) shows the maximum principal strain distribution at the maximum negative load. After flexural cracks occurred in the columns and beams in the early stage of loading, diagonal cracks were observed connecting the corner and corner sections. The diagonal cracks were generated and propagate simultaneously.

Figure 3(b) shows the minimum principal stress distribution at the maximum negative load. A compression strut was formed along the diagonal crack from the corner to the bending of the outer axial rebar. When the inner radius in bending was small (=3ϕ), the compression damage of concrete occurred at the inner radius in bending because the area that bears the compressive force was small. On the other

hands, when the inner radius in bending was large (=10ϕ), the width of the compression strut was also increased, and the failure was assumed to occur at the corner where the compression area was relatively small.

4.3 T-shape case

Figure 2(c) shows the maximum principal strain distribution at the maximum load and Figure 3(c) shows the minimum principal stress distribution at the maximum load. Based on the relationship between the location of cracks and the directions of loading and the compression strut, the trend was similar to that of the positive loading of the L-shaped joints.

5 EVALUATIONS OF JOINTS BY DAMAGE INDICES

5.1 Application of Damage Indicators to Joints

The initiation of diagonal cracking and the compression damage at the joint were evaluated using the damage indices $\sqrt{J_2'}$ =1000μ and $\overline{W_n}$=1500μ. The L-shaped case was divided into three members, such as column, beam, and the joint. The T-shaped case was divided into four members, such as column, right and left beams, and joint. The maximum values of damage index $\sqrt{J_2'}$ and $\overline{W_n}$ in each member were calculated. The relationship between displacement and the damage index obtained by calculating the maximum value in the specified area are called J-curve and W-curve in this paper.

(1) L-shaped model with positive loading

Figure 4 shows the load-displacement curve, the J-curve and the W-curve at the joint. Each figure also shows the value of the W-curve of the joint at the maximum load $\overline{W_n}_{\mathrm{pmax}}$.

Figure 5 shows the distribution of $\sqrt{J_2'}$ and the maximum principal strain when the J-curve of the joint reaches 1000μ in the L-1.0-P3 and L-1.6-P3. The $\sqrt{J_2'}$ evaluated the cracks occurred along the axial rebar in all cases. Figure 4 indicates that the effect of the inner radius of bending on the J-curve was small.

Figure 6 shows the distribution of $\overline{W_n}$ and the minimum principal stress when the W-curve reached 1500μ for the L-1.0-P3 and L-1.6-P3, and the minimum principal stress at the maximum load for the L-1.6-P3. The distribution of $\overline{W_n}$ and the minimum principal stress for the case with an inner radius in bending of 10ϕ were generally similar to those for the case with 3ϕ. Figure 6 shows that when H/B=1.0, the W-curve was roughly equivalent at $\overline{W_n}$ reaching 1500μ and at the maximum load. The value of $\overline{W_n}$ exceeded 1500μ at both ends of the compression strut, which was consistent with the expected damage pattern at H/B=1.6, W-curve reached 1500μ prior to the maximum load.

Figure 6 also indicates that when only the elements at the surface reached 1500μ, none of the inner elements reached 1500μ. In other words, the maximum load was considered to be

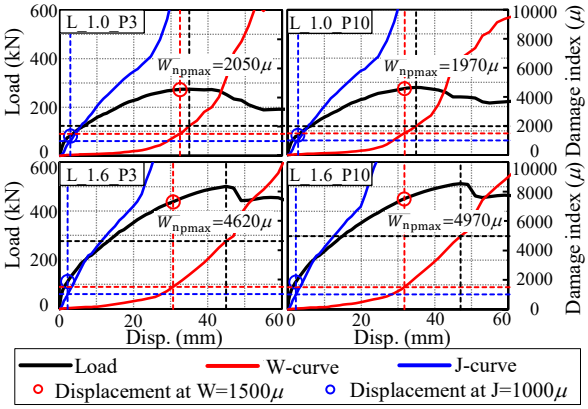

Figure 4 L-shaped model. (loading in positive)

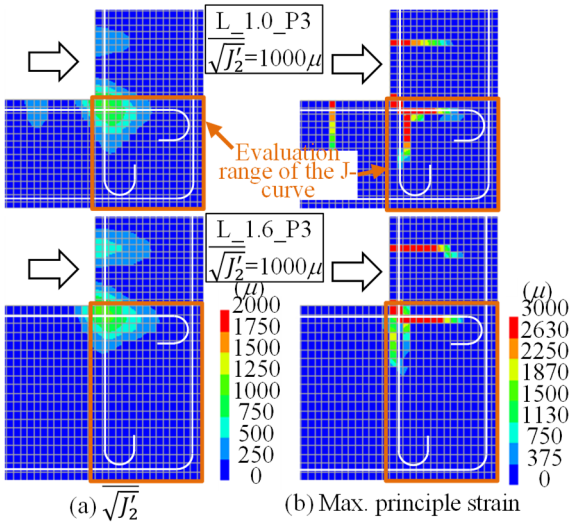

Figure 5 L-shaped model. (loading in positive)

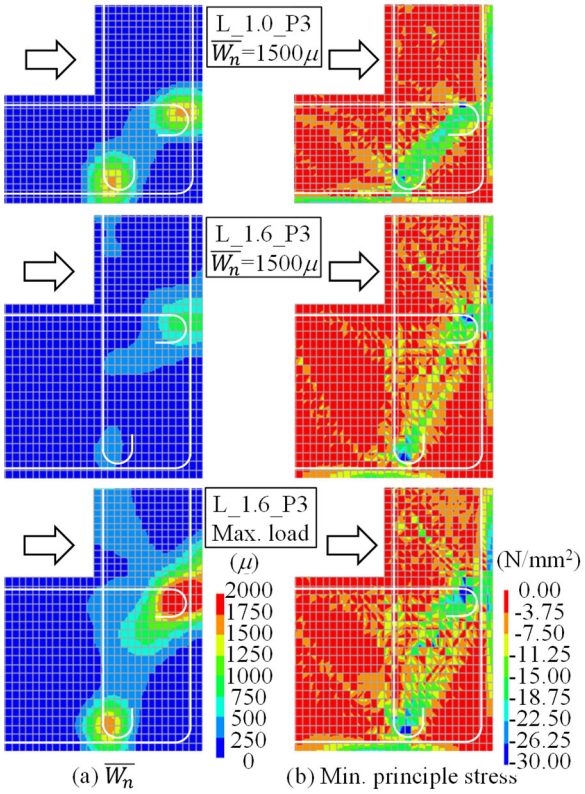

Figure 6 L-shaped model. (loading in positive)

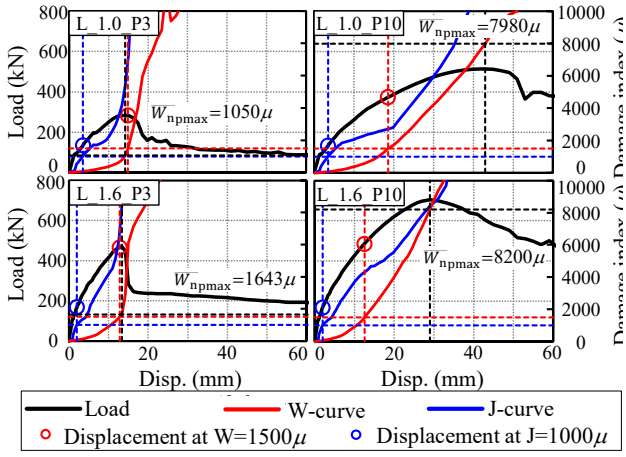

Figure 7 L-shaped model. (loading in negative)

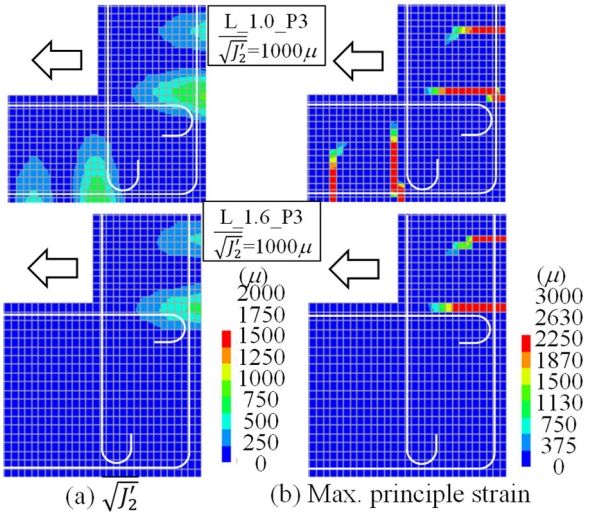

Figure 8 L-Shaped model. (loading in negative)

taken when $\overline{W_n}$ of the inner elements as well as the surface elements reached 1500μ. It can also be seen that the damage was preceded at the base of the column, which was a relative weak point due to the increased beam height.

(2) L-shaped model with negative load

Figure 7 shows the load-displacement curve, J-curve at the joint, the W-curve at the joint. Each figure also shows the value of the W-curve at the joint at maximum load $\overline{W_{n\text{pmax}}}$. Figure 8 shows the distribution of $\overline{\sqrt{J_2'}}$ and the maximum principal strain when the J-curve reaches 1000μ for L-1.0-P3 and L-1.6-P3. The flexural cracks at the base of columns and beams are evaluated in both cases. The distribution of $\overline{\sqrt{J_2'}}$ indicates that the effect of the inner radius of bending on the flexural cracks was small, however, the trend of the J-curve differs with the size of the inner radius of bending as the displacement increases, which was due to differences in the propagation of diagonal cracks.

Figure 9 shows the distribution of $\overline{W_n}$ and the minimum principal stress when the W-curve reaches 1500μ in the L-shaped case. When the inner radius in bending was 3ϕ, the $\overline{W_n}$ reached 1500μ at the inner radius in bending and the maximum load was almost the same. And the $\overline{W_n}$ reaches 1500μ at the inner radius in bending with case of H/B=1.0. This is consistent with the expected damage pattern. On the other hands, $\overline{W_n}$ reached 1500μ even at the corner with the case of H/B=1.6,, suggesting that the damage at the column base, which was a relative weak point, occurred at the same time as the damage at the joint. Although the W-curve reaches 1500μ prior to the maximum load when the inside radius in bending was 10ϕ. It means that the damage occurred at the corner.

(3) T-shape case

Figure 10 shows the load-displacement curve, the J-curve at the joint, and the W-curve

at the joint. Each figure also shows the value of the W-curve at the joint at maximum load $\overline{W_{n\,\mathrm{pmax}}}$. Figure 11 shows the distribution of $\sqrt{J_2'}$ and the maximum principal strain when the J-curve reaches 1000μ for the T-1.0 and T-1.6. The flexural crack in the column members was evaluated by using the index in both cases.

Figure 12 shows the distribution of $\overline{W_n}$ and the minimum principal stress when the W-curve reaches 1500μ for the T-1.0 and T-1.6. The case of H/B=1.0 and H/B=1.6 for the T-joints show the same trend as that for the positive loading of H/B=1.0 and H/B=1.6 for the L-shaped model, respectively. The load-bearing capacity was, however, about 10% to 20% lower than that of the L-shaped case under positive loading. This indicates that the distribution of $\overline{W_n}$ or the minimum principal stress of the T-shape case was similar to the distribution of $\overline{W_n}$ and the minimum principal stress of the L-shape case under positive loading with the same H/B.

The joint damage was generally evaluated by $\overline{W_n}$=1500μ for both negative and positive loading in the L-shaped model, while the T-shaped model shows the same damage pattern as the positive loading in the L-shaped model. If the limit value of $\overline{W_n}$=1500μ was neglected, it was suggested that the point at which the W-curve begins to increase rapidly, as seen in Figure 5, Figures 8 and 10 was determined as the point corresponding to the maximum load at the joint. The point at which the W-curve begins to increase rapidly, as seen in Figures 4, 8, and 10, were determined as the point corresponding to the maximum load on the joint.

5.2 Evaluation by subdivision of joints

In 5.1, the arrival of the J-curve at 1000μ at the joints corresponded to the occurrence of flexural cracks to the base of the columns and beams. In the case of damage at corner angles of the L-shaped model, the damage was determined earlier than in other cases. To verify the applicability of $\sqrt{J_2'}$ and $\overline{W_n}$ to diagonal cracks and damage at corner corners, $\sqrt{J_2'}$ and $\overline{W_n}$ were extracted for each joint location and examined. Figure 13 shows the location of each

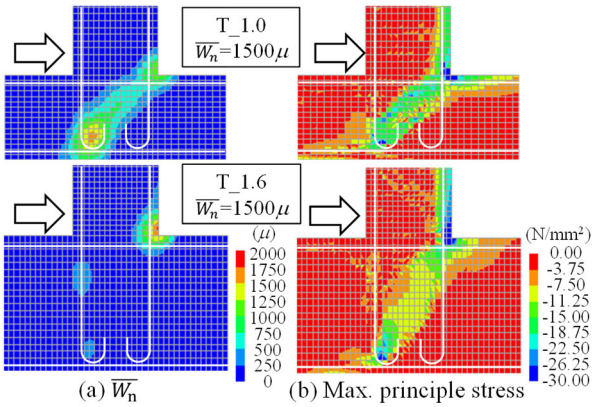

Figure 12 T-shaped model. (loading in positive)

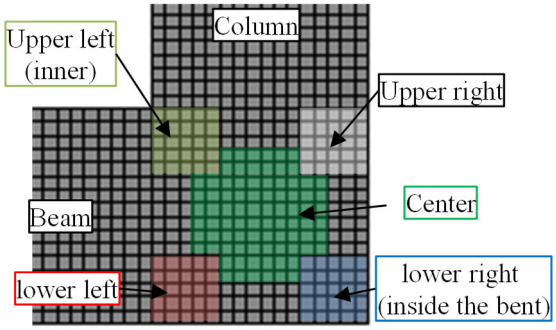

Figure 13 Parts in joint.

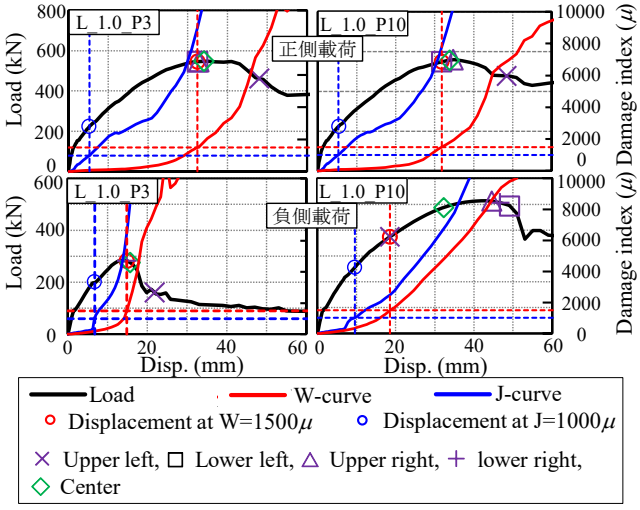

Figure 14 Damage indexes at parts in joints.

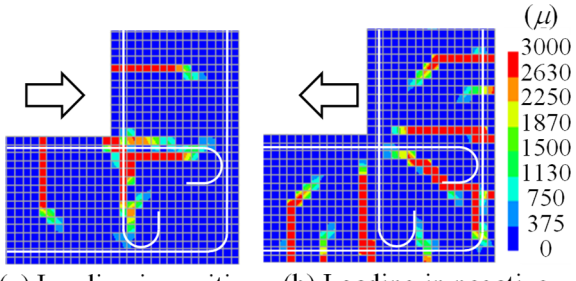

Figure 15 Max. principal strain when center of the joint $\overline{W_n}$=1500 μ.

part. Since diagonal cracks occur in the center of the joint (center) and damage occurs at the corner (upper left), inner radius of bending (lower right), and near the base of columns (upper right) and beams (lower left), the division method was used to distinguish between them based on the results of the present analysis.

The reason for early damage determination in the case of damage at corner angles was that the damage at corner angles was a multi-axial compressive stress field subjected to compressive struts and flexural compressive stresses in the columns and beams. Although there are some possible solutions to this problem, such as changing the limit value of the damage index or the averaging length, this study applied the same value that decided by RC beams, and focus on the locations in the joint. The occurrence of diagonal cracks and the location of damage were evaluated.

Figure 14 shows the load-displacement curve, J-curve, and W-curve. since the diagonal cracks occurring in the joint are to be determined, the J-curve shows the curve at the center of the joint, the W-curve shows the curve at the joint as in 5.1, and the displacement at which the W-curve reaches 1500μ at each site within the joint is plotted.

Figure 15 shows the maximum principal strain distribution when the J-curve in the center of the joint reached 1000μ in the L-1.0-P3. In all loading directions, the maximum principal strain distribution is immediately after diagonal cracking occurs, and $\overline{\sqrt{J_2'}}$=1000μ was evaluated as the limit value by focusing on the point where diagonal cracking occurs.

The damage at each loading direction is as follows.

(1) When loaded on the positive side

From Figure 14, the compression strut was damaged at both ends because the W-curves at the upper right or lower left of the joint reached 1500μ and at the maximum load were the same. This was also evident from Figure 6.

(2) Negative Loading

Figure 14 shows that in the case of L-1.0-P3, damage was considered to have occurred at the lower right end of the compression strut (inside radius of bending), because the W-curve at the lower right of the joint reached 1500μ and the maximum load was almost the same. The maximum load was taken when the damage at the upper left end of the compression strut (corner corner) developed to the lower right end (inner radius of bending).

6 CONCLUSIONS

By dividing the joint into sections and restricting the evaluation to the area where the target crack occurs, and by using $\overline{\sqrt{J_2'}}$, the diagonal cracks in the joint was evaluated by $\overline{\sqrt{J_2'}}$=1000μ even if the model used the discrete rebar. The L-shape and T-shape cases were used to evaluate the diagonal cracks at the joints. By dividing the L-shape and T-shape cases and evaluating them by the damage index $\overline{W_n}$, it was found that the joint damage was evaluated approximately by $\overline{W_n}$=1500μ even for models using discrete bars.

Cases of damage at corner angles, which are multiaxial compressive stress fields, were determined earlier than other cases. By examining each site separately, the maximum load was taken when $\overline{W_n}$=1500μ at the inner radius of bending.

ACKNOWLEDGEMENTS

This study was partially supported by a grant from the Ministry of Land, Infrastructure, Transport and Tourism for the development of railway technology.

REFERENCES

[1] Japan Society of Civil Engineers, 2017. *Standard Specification for Concrete Structures-2017 (Design Edition)*. Maruzen.

[2] Saito, S., Maki, T., Tsuchiya, S. and Watanabe, T. 2011. Damage assessment of RC beams by nonlinear finite element analyses. *J. of JSCE E2*. **67**(2): 166-180.

[3] Kusano, H, Nakata, Y., Tadokoro, T., and Abo, T., 2018. Influence of Reinforcement Specification in Joint on Fracture

Properties of L-Shaped RC Column-Beam Joint, *15th Japan Earthquake Engineering Symposium*. 51-60.

[4] Nishimura, S., Nakata, Y., Watanabe, K., Tadokoro, T. and Abo, T. 2020. Study on Damage Process and Evaluation by Analysis of T-Shaped Beam-Column Joints with Equal Cross Section Height. *75th Annual Conference of JSCE*, V-602.

[5] Matsumoto, T., Higai, I. and Saito, S. 2004. Experimental Study on Effect of Cover Thickness on Adhesion Properties of Deformed Bars. *Proc. of the Japan Concrete Institute*. 26(2). 823-828.